

# Simultaneous Determination of the Size and Surface Charge of Individual Nanoparticles Using a Carbon Nanotube-Based Coulter Counter

Takashi Ito, Li Sun, and Richard M. Crooks\*

Department of Chemistry, Texas A&M University, P.O. Box 30012, College Station, Texas 77842-3012

**A resistive-pulse Coulter counter based on a membrane containing a single multiwall carbon nanotube (MWNT) channel was used to simultaneously determine the size and surface charge of carboxy-terminated polystyrene nanoparticles. The membrane was prepared from an epoxy section containing a MWNT channel mounted on a poly-(dimethylsiloxane) (PDMS) support structure. The PDMS support reduced the background noise level by a factor of >20 compared to the Si/Si<sub>3</sub>N<sub>4</sub> support structure used in our previous study. The lower noise level makes it possible to accurately measure the height and width of resistive-pulse signals resulting from transport of individual particles through the MWNT channel. Particle sizes, calculated from current pulse heights, were comparable to those determined by transmission electron microscope (TEM). The width of the current pulses is a measure of the nanoparticle transport time, and it permits calculation of the electrokinetic surface charge. Different types of polystyrene nanoparticles having nearly the same size, but different electrokinetic surface charge, could be resolved on the basis of the difference in their transport time.**

Here we report the simultaneous determination of the size and surface charge of individual acid-functionalized nanoparticles using a resistive-pulse (Coulter) counter based on a single 130-nm-diameter pore defined by a multiwall carbon nanotube (MWNT). The experimental apparatus used in this study provides improved performance as compared to our previous report of a MWNT-based Coulter counter.<sup>1</sup> Specifically, this new approach results in a greatly improved signal-to-noise (S/N) ratio and better time resolution. Accordingly, it is now possible to accurately measure the true height and width of pulse signals corresponding to transport of individual particles through a MWNT channel.

Coulter particle counters have been used to count and analyze many different types of particles, ranging from biological cells to colloidal particles.<sup>2,3</sup> A typical Coulter counter consists of a single small pore (typically 5  $\mu\text{m}$ –2 mm in diameter) that separates two electrolyte solutions. A constant potential is applied across the

sensing pore, and the resulting ion current is continuously monitored. Transport of analyte particles through the pore results in an increase in the pore resistance, and the corresponding decrease in the ion current can be detected. The magnitude of the current decrease correlates to the size of the analyte particles, and its duration is related to the residence time of the analyte in the pore. The number of such current pulses can be related to the analyte concentration. The principles governing this detection strategy predict that smaller sensing pores permit detection of smaller particles.<sup>2,3</sup>

In the 1970s, DeBlois et al. reported the detection of viruses (~100 nm in diameter) using a track-etched polycarbonate membrane containing a single, 450-nm-diameter pore.<sup>4,5</sup> In 1990s, research groups led by Branton and Bayley reported molecular Coulter counters based on porous membrane proteins having a diameter of ~2 nm.<sup>3,6</sup> With these very small channels, they were able to detect individual metal ions, small organic molecules, and even single-strand DNA. Very recently, Branton's group used ion-milling to fabricate artificial pores (5-nm diameter) in a Si<sub>3</sub>N<sub>4</sub> substrate, and the device based on this approach allows counting of 500 bp, double-strand DNA.<sup>7</sup> Finally, Saleh and Sohn demonstrated that a 200-nm-diameter pore fabricated in poly(dimethylsiloxane) (PDMS) permits detection of Lambda-phage DNA using the Coulter counting principle.<sup>8</sup>

We previously reported a Coulter counter constructed with a membrane containing a single MWNT. This device permitted measurements of polystyrene nanoparticles having diameters in the range 60–100 nm.<sup>1</sup> Statistical data analysis of the frequency of particle transport provided quantitative information on hydrodynamic and electrophoretic mass transport rates. However, the S/N ratio of this system was not very good, and this resulted in a transport time resolution of only ~1 ms. Here, we show that the S/N ratio and, as a result, the time resolution of the Coulter counter have been substantially improved by replacing the Si/Si<sub>3</sub>N<sub>4</sub> membrane support structure used in our previous work with one fabricated from PDMS, which has superior electrical properties.<sup>9</sup> The immediate benefit of this approach is that both the size

\* To whom correspondence should be addressed. Phone: 979-845-5629. Fax: 979-845-1399. E-mail: crooks@tamu.edu.

(1) Sun, L.; Crooks, R. M. *J. Am. Chem. Soc.* **2000**, *122*, 12340–12345.

(2) Lines, R. W. In *Particle Size Analysis*; Stanley-Wood, N. G., Linew, R. W., Eds.; Royal Society of Chemistry: Cambridge, 1992; pp 351–383.

(3) Bayley, H.; Martin, C. R. *Chem. Rev.* **2000**, *100*, 2575–2594.

(4) DeBlois, R. W.; Bean, C. P. *Rev. Sci. Instrum.* **1970**, *41*, 909–916.

(5) DeBlois, R. W.; Wesley, R. K. A. *J. Virol.* **1977**, *23*, 227–233.

(6) Deamer, D. W.; Branton, D. *Acc. Chem. Res.* **2002**, *35*, 817–825.

(7) Li, J.; Stein, D.; McMullan, C.; Branton, D.; Aziz, M. J.; Golovchenko, J. A. *Nature* **2001**, *412*, 166–169.

(8) Saleh, O. A.; Sohn, L. L. *Nano Lett.* **2003**, *3*, 37–38.

(9) Klemic, K. G.; Klemic, J. F.; Reed, M. A.; Sigworth, F. J. *Biosens. Bioelectron.* **2002**, *17*, 597–604.

and the surface charge of individual particles can now be accurately measured. We also show that polystyrene nanoparticles having nearly the same size but different surface charge can be distinguished in mixed solutions of varying composition. The improved S/N level also brings us closer to our goal of using carbon nanotubes having even smaller diameters to directly detect large molecules, such as polymers and DNA.

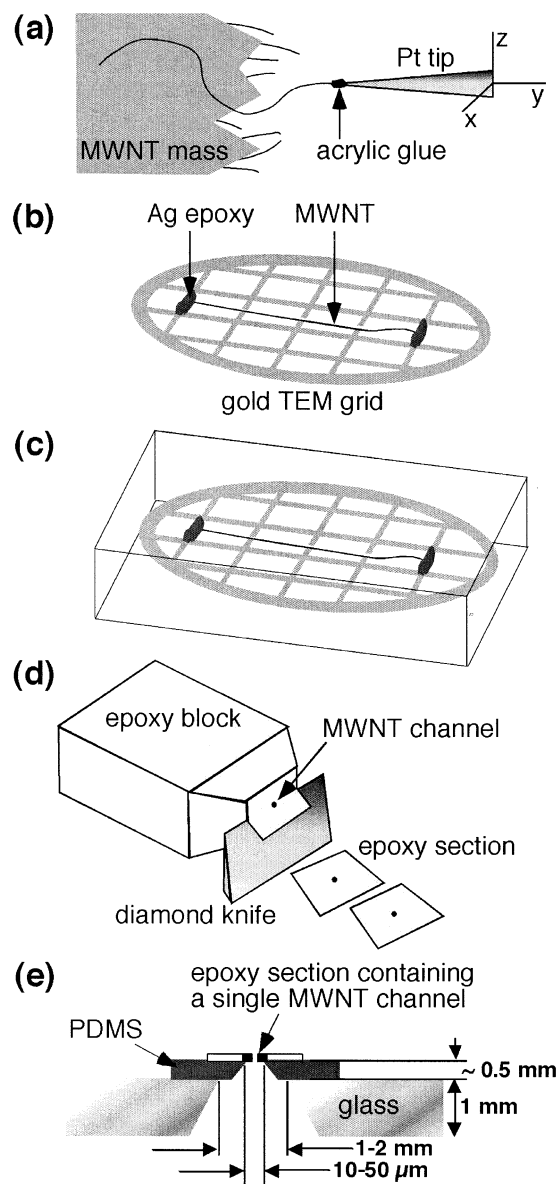
## EXPERIMENTAL SECTION

**Chemicals and Materials.** All solutions were prepared with water having a resistance of 18.2 M $\Omega$  cm (Milli-Q, Millipore) and filtered through a 0.2- $\mu$ m membrane filter (Fisher Scientific, Pittsburgh, PA). KCl (EM Sciences, Gibbstown, NJ), Triton X-100, and NaClO<sub>4</sub> (Sigma Chemical, St. Louis, MO), KH<sub>2</sub>PO<sub>4</sub> and K<sub>2</sub>HPO<sub>4</sub> (Mallinckrodt Chemical, Paris, KY), and pyrrole (Aldrich, Milwaukee, WI) were of reagent grade quality or better and were used without further purification. Multiwall carbon nanotubes (Applied Sciences Cedarville, OH)<sup>10,11</sup> were prepared via a chemical vapor deposition process. Polystyrene nanospheres having a low (IDC-PS, 57  $\pm$  6-nm diameter, 120 -COOH functional groups per particle; from Interfacial Dynamics, Portland, OR) and high (Bangs-PS, 60  $\pm$  10-nm diameter, 24 220 -COOH functional groups per particle; from Bangs Laboratories, Fishers, IN) acid surface density were used as received. The manufacturers indicate that the particle size and number density of acid groups were determined by TEM and conductometric titration, respectively.

**Fabrication of Membranes Containing a Single MWNT Channel.** Single MWNT channels were fabricated as shown in Scheme 1.<sup>1</sup> An *xyz*-translation stage (model 462, Newport, Irvine, CA) attached to an optical microscope (100–600 $\times$  magnification, Optiphot, Nikon, Tokyo) was used to perform the following manipulations. A single MWNT was removed from a bundle using a sharp Pt tip having acrylic adhesive (adhesive carbon tape, Ted Pella Inc., Redding, CA) on its apex (frame a of Scheme 1). Before the MWNT was mounted onto a Au TEM grid (T200Au, Electron Microscopy Sciences or EMS, Fort Washington, PA) and immobilized with Ag epoxy (Epotek H20E, Epoxy Technology, Billerica, MA) (frame b of Scheme 1), one end of the nanotube was electrochemically modified with polypyrrole using an aqueous electrolyte solution containing 0.1 M NaClO<sub>4</sub> + 0.1 M pyrrole, by repeated scanning at 0.1 V/s scan rate between 0 and +1.2 V vs Ag/AgCl.<sup>11</sup> Polypyrrole modification closes one end of the nanotube while keeping the tube interior open (data not shown).<sup>12</sup> This results in a high yield of useable MWNT membranes, because uncapped MWNTs were nearly always filled by Ag epoxy (11 out of 11 samples examined) when the MWNTs were immobilized on the Au TEM grid, but more than half of polypyrrole-capped MWNTs had open pores (11 out of 20 samples; see Supporting Information for TEM images).

MWNTs immobilized on Au TEM grids were embedded in an epoxy matrix (Epo-Fix, EMS) (frame c of Scheme 1), and the resulting epoxy block was microtomed (UltraCut E, Reichert-Jung) to yield trapezoid-shaped sections ( $\sim$ 1  $\times$   $\sim$ 1 mm) that were  $\sim$ 1  $\mu$ m in thickness (frame d of Scheme 1). The pore diameter of the

Scheme 1



MWNT channels was found to be 132 nm according to TEM measurements (JEOL JEM-2010) calibrated against a grating-replica size standard (Electron Microscopy Sciences, TEM images shown in Supporting Information). A section containing a single nanotube channel was mounted on a thin (0.5-mm thickness), circular (5-mm diameter) PDMS (Sylgard 184, Dow Corning, Midland, MI) support structure containing a square hole (10–50- $\mu$ m edge length). The support structure,<sup>9</sup> in turn, was immobilized on a glass substrate ( $\sim$ 12  $\times$  12 mm) containing a cylindrical, sand-blasted hole ( $\sim$ 2 mm diameter), as shown in frame e of Scheme 1.

**Cell Configuration and Data Acquisition.** The cell configuration used here was the same as that described in our previous report.<sup>1</sup> A section mounted on a PDMS/glass support was clamped between two half cells fabricated from polycarbonate and sealed with a silicone O-ring. The cell was placed in a Faraday cage on a vibration isolation table (model AS-130, TMC, Peabody, MA). Current was measured in voltage-clamp mode with an integrated data acquisition system (Axopatch 200B and Digipack 1200, Axon

(10) Campbell, J. K.; Sun, L.; Crooks, R. M. *J. Am. Chem. Soc.* **1999**, *121*, 3779–3780.

(11) Ito, T.; Sun, L.; Crooks, R. M. *Electrochem. Solid-State Lett.* **2003**, *6*, C4–C7.

(12) Chen, J. H.; Huang, Z. P.; Wang, D. Z.; Yang, S. X.; Wen, J. G.; Ren, Z. F. *Appl. Phys. A* **2002**, *73*, 129–131.

Instruments, Foster City, CA). Ag/AgCl electrodes were dipped in both half cells. Sometimes air bubbles would block the channel, but these could be removed under reduced pressure.<sup>13</sup> Prior to carrying out Coulter counting measurements, a cyclic voltammogram (CV) of the channel was obtained in a solution containing 0.1 M KCl, 0.01 M KH<sub>2</sub>PO<sub>4</sub>/K<sub>2</sub>HPO<sub>4</sub> (pH 7.3), and 0.1% (w/v) Triton X-100. For this measurement, a Pine Instruments model AFRDES bipotentiostat (Grove City, PA) was used to generate the voltage ramp, and the current was measured with the Axopatch 200B. The channel length ( $l_c$ ) can be calculated using the CV data and eq 1.<sup>4</sup>

$$S_c = \frac{i_c}{E_M} = \frac{\kappa\pi d_c^2}{4(l_c + 0.8d_c)} \quad (1)$$

Here,  $S_c$  is the ionic conductivity of the channel,  $i_c$  is the measured ionic current upon application of membrane potential  $E_M$ ,  $d_c$  is the channel diameter, and  $\kappa$  is the electrolyte conductivity. The factor of  $0.8d_c$  corrects for the so-called “end effect”, which becomes significant when the pore diameter is comparable to the pore length. Coulter counting measurements were made by replacing the electrolyte solution in the side of the cell held at ground with a solution of polystyrene nanospheres ( $5 \times 10^{11}$  particles/mL, 0.1 M KCl, 0.01 M KH<sub>2</sub>PO<sub>4</sub>/K<sub>2</sub>HPO<sub>4</sub> (pH 7.3), and 0.1% w/v Triton X-100). The data provided in this paper were obtained with MWNT channels having a diameter of 132 nm and a length of 0.94  $\mu\text{m}$ ; MWNT channels having the same diameter and different lengths (0.83–1.21  $\mu\text{m}$ ) gave very similar results. Current vs time traces were collected with the AxoScope 8.0 (Axon Instruments) using a 10- $\mu\text{s}$  sampling interval, a 10-kHz lowpass Bessel filter, and no digital filtering. The data were processed using custom-written software.<sup>1</sup>

## RESULTS AND DISCUSSION

**Enhancing the S/N Ratio of Coulter Counter Data.** In our previous study,<sup>1</sup> low-pass analogue and digital filters were used to remove electronic noise from the Coulter current signal. The cutoff frequency of the combined filters was not very high, so the time resolution of the transport measurements was limited to  $\sim 1$  ms. This made it difficult to accurately determine the height and width of current pulses corresponding to nanosphere transport through the MWNT channels. We attributed this difficulty to the presence of charge carriers in the Si/Si<sub>3</sub>N<sub>4</sub> support structure, which is used to lend mechanical strength to the epoxy section housing the MWNT channel. Accordingly, we examined PDMS as an alternative material for supporting the epoxy section.<sup>14</sup> An additional advantage of PDMS is that many support structures can be easily prepared via a molding process using a common master template.<sup>9</sup>

Figure 1a and b show background currents at membrane potentials ( $E_M$ ) of 0 V for MWNT channels attached to support structures composed of Si/Si<sub>3</sub>N<sub>4</sub> and PDMS, respectively. The peak-to-peak (p–p) noise obtained using the PDMS support was  $< 10$  pA for a 10- $\mu\text{s}$  sampling time using a 10-kHz analogue Bessel

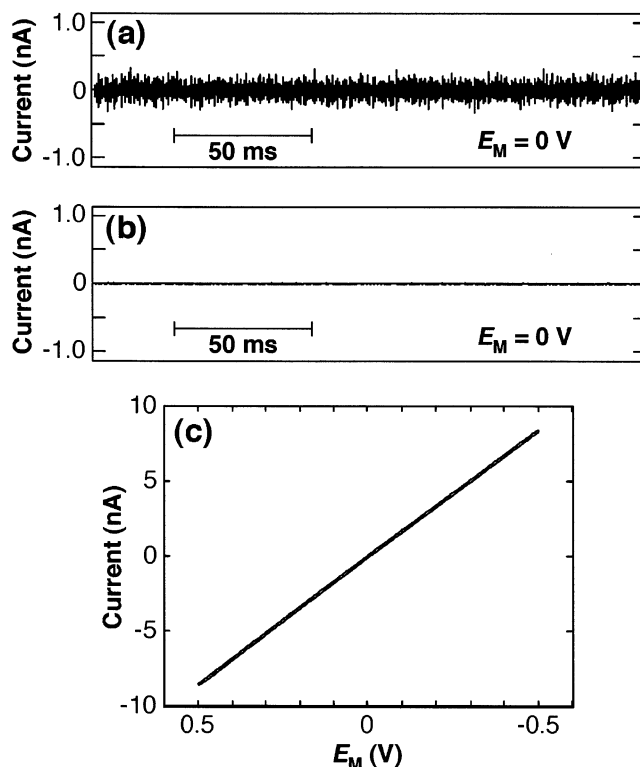


Figure 1. Plot of current vs time showing baseline currents at  $E_M = 0$  V for a MWNT channel on (a) a Si/Si<sub>3</sub>N<sub>4</sub> and (b) a PDMS support structure in a solution containing 0.1 M KCl, 10 mM KH<sub>2</sub>PO<sub>4</sub>/K<sub>2</sub>HPO<sub>4</sub> buffer (pH 7.3), and 0.1% (w/v) Triton X-100. Sampling time, 10  $\mu\text{s}$ ; low-pass Bessel filter, 10 kHz; and no digital filtering. (c) Typical cyclic voltammogram of an MWNT channel on a PDMS support structure in an electrolyte having the same composition as in (a) and (b). Scan rate: 0.1 V/s. The slope yields a channel length of 939 nm.

filter, which is intrinsic to the Axopatch 200B amplifier.<sup>15</sup> The instrument manufacturer also provides a digital filter, but further filtering with a 10-kHz digital filter does not change the signal. Thus, in this study, digital filtering was not used. In contrast, the p–p noise measured using the Si/Si<sub>3</sub>N<sub>4</sub> support was  $> 200$  pA when identical filtering was used. For 60-nm-diameter polystyrene spheres, the typical pulse signal is  $< 200$  pA at  $E_M = +0.5$  V (vide infra); therefore, signal detection using the Si/Si<sub>3</sub>N<sub>4</sub> support is nearly impossible without decreasing the cutoff frequency of the analogue or digital filters. Excessive filtering, however, distorts the shape of the current pulses. The lower noise observed for the PDMS support is attributable to the low capacitance of this material.<sup>14</sup> Figure 1c is a typical CV for a MWNT channel supported on PDMS. The capacitance of this sample, as calculated from  $\Delta i/2v$  (where  $v$  is the scan rate and  $\Delta i$  is the height of the hysteresis loop in the CV), is 0.5 nF, which is 10 to 15 times smaller than the value for the Si/Si<sub>3</sub>N<sub>4</sub> support (5–7.5 nF).<sup>1</sup>

**Coulter Counting of Polystyrene Particles Having Low Surface–COOH Density.** To demonstrate that a MWNT-based Coulter counter can simultaneously determine the size and charge of acid-functionalized polystyrene spheres, we examined the transport properties of a sample that was well characterized by the vendor using traditional methods. Specifically, these spheres (IDC-PS) have a diameter of  $57 \pm 6$  nm and 120 –COOH

(13) Monahan, J.; Gewirth, A. A.; Nuzzo, R. G. *Anal. Chem.* **2001**, *73*, 3193–3197.

(14) Levis, R. A.; Rae, J. L. *Methods Enzymol.* **1998**, *293*, 218–266.

(15) Sherman-Gold, R. *The Axon Guide for Electrophysiology & Biophysics Laboratory Techniques*; Axon Instruments: Foster City, CA, 1993.

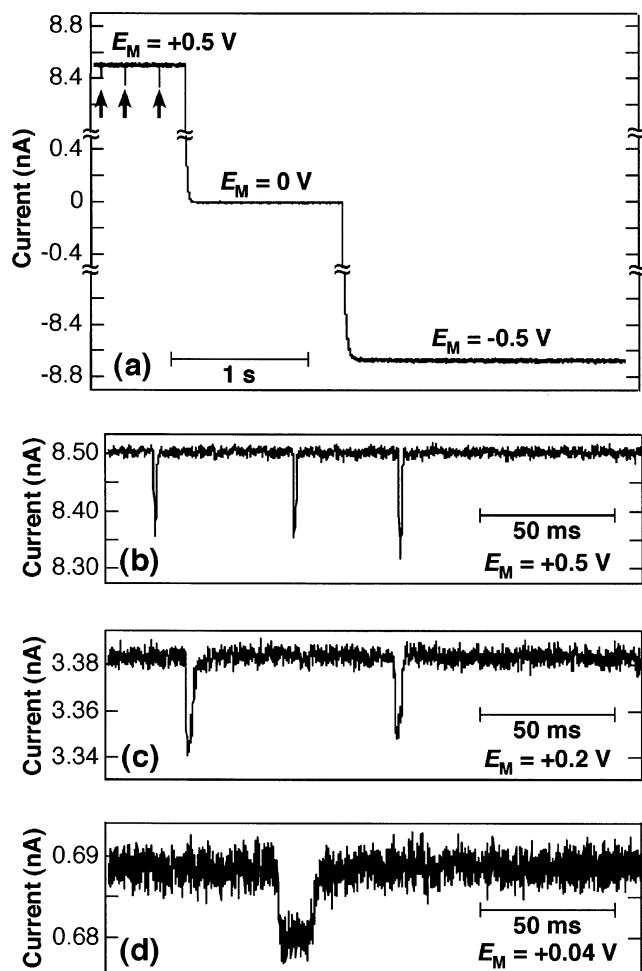


Figure 2. (a) Plot of current vs time for potential steps of  $E_M = +0.5$ , 0, and  $-0.5$  V obtained using a solution containing nominally  $5 \times 10^{11}$  IDC-PS particles/mL, 0.1 M KCl, 10 mM  $\text{KH}_2\text{PO}_4/\text{K}_2\text{HPO}_4$  buffer (pH 7.3), and 0.1% (w/v) Triton X-100. The MWNT channel is 939 nm long and 132 nm in diameter. (b–d) High-resolution plots of current vs time obtained at  $E_M = +0.5$ ,  $+0.2$ , and  $+0.04$  V, respectively. Other conditions were the same as in (a).

functional groups per particle. Figure 2a shows a plot of current vs time for IDC-PS nanoparticles at  $E_M = +0.5$ , 0, and  $-0.5$  V. Current pulses (indicated by arrows) were observed only at positive potentials, and as  $E_M$  decreases, the pulse width increases and counting frequency decreases (Figure 2b–2d). This trend is represented more quantitatively in Figure 3a, which is a distribution plot of the number of current pulses as a function of transport time ( $\Delta t$ ). The averages and the standard deviation of  $\Delta t$  are given in Table 1.

The data in Figures 2 and 3 are consistent with transport by either electrophoresis or electroosmosis. However, electroosmotic transport requires that the inner wall of the nanotube channel support immobile positive charges. Consistent with chemical intuition, previous streaming potential measurements have shown that the nanotube interiors are charge-neutral.<sup>1</sup> Accordingly, electrophoresis is the dominant transport mode, and therefore, the transport time can be linked directly to the electrophoretic mobility,  $\mu$ , by its definition, which is the average particle speed per unit field gradient (eq 2).<sup>16</sup>

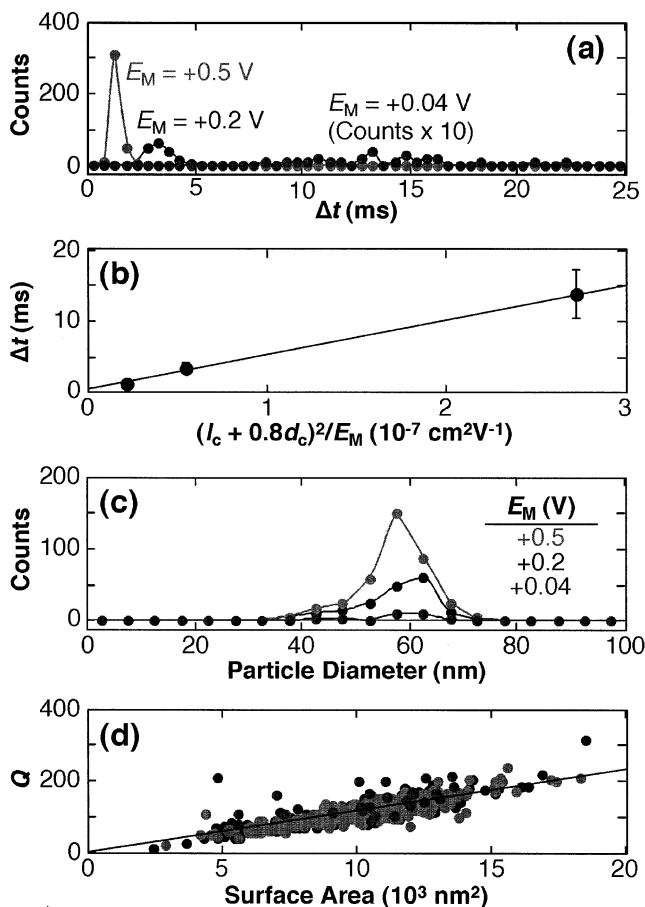


Figure 3. Characteristic transport parameters for the IDC-PS probe particles at membrane potentials ( $E_M$ ) of  $+0.5$ ,  $+0.2$ , and  $+0.04$  V. (a) Distribution of particle transport times ( $\Delta t$ ). (b) Relationship between  $(I_c + 0.8d_c)^2/E_M$  and  $\Delta t$ . The solid line is the best fit. (c) Distribution of particle diameters calculated from the pulse heights. (d) Total electrokinetic surface charge ( $Q$ ), calculated using eq 4, as a function of particle surface area. The solid line is the best fit, and its slope provides the average surface charge per area, which in turn relates to the average number of charges per particle. The total analysis times were different at the three membrane potentials (Table 1).

Table 1. Diameter, Transport Time, Electrokinetic Surface Charge, and Counting Frequency for IDC-PS Probes Determined from Coulter Counting Data

$E_M$ (V)	$N^a$ (time, s) <sup>e</sup>	$d_s$ (nm) <sup>b,c</sup>	$\Delta t$ (ms) <sup>c</sup>	$Q^d$	$J_s$ (s <sup>-1</sup> )
0.04	26 (121.4)	$58.6 \pm 7.5$	$13.8 \pm 3.4$	$150 \pm 50$	0.21
0.2	180 (118.9)	$57.0 \pm 7.8$	$3.4 \pm 0.7$	$120 \pm 40$	1.51
0.5	377 (84.5)	$57.2 \pm 6.5$	$1.3 \pm 0.2$	$120 \pm 30$	4.46

<sup>a</sup> Total number of current pulses measured. <sup>b</sup> Particle diameter calculated using eq 5. <sup>c</sup> Average standard deviation. <sup>d</sup> Electrokinetic surface charge per particle calculated from eq 4. <sup>e</sup> Total time for each measurement.

$$\mu = \left( \frac{I_c + 0.8d_c}{\Delta t} \right) \left( \frac{E_M}{I_c + 0.8d_c} \right)^{-1} = \frac{(I_c + 0.8d_c)^2}{E_M \Delta t} \quad (2)$$

Figure 3b indicates that transport through the MWNT channel obeys this relationship and that a plot of  $\Delta t$  vs  $(I_c + 0.8d_c)^2/E_M$  is linear; the slope yields an electrophoretic mobility of  $2.1 \times 10^{-5} \text{ cm}^2 \text{ V}^{-1} \text{ s}^{-1}$ . The electrophoretic mobility is linked to the surface

charge  $Q$  according to eq 3.<sup>16</sup>

$$\mu = \frac{Q}{2\pi\eta d_s(1 + d_s/2d_D)} \quad (3)$$

Here,  $\eta$  is the viscosity of the solution,  $d_D$  the Debye length ( $\sim 1$  nm for a 0.1 M 1:1 electrolyte solution),<sup>17</sup> and  $d_s$  the particle diameter. It should be noted that eq 3 is derived by combining the Helmholtz–Smoluchowski equation and the Debye–Hückel approximation; thus, it is applicable only to the case where the particle size is much larger than the electrical double layer and the surface  $\zeta$  potential is small so that the Poisson–Boltzmann equation can be linearized. Equation 4, which is derived by combining eqs 2 and 3, shows that once the diameter of a particle is determined from the height of a current pulse (vide infra),  $Q$  for the particle can be readily calculated using the width,  $\Delta t$ , of the same pulse.

$$Q = \frac{2\pi\eta(I_c + 0.8d_c)^2 d_s(1 + d_s/2d_D)}{E_M \Delta t} \quad (4)$$

The ratio between the pulse height ( $\Delta i_c$ ) and the steady-state baseline current gives the diameter of a particle passing through the channel (eq 5).<sup>4</sup>

$$\frac{\Delta i_c}{i_c} = S(d_c, d_s) \frac{d_s^3}{(I_c + 0.8d_c)d_c^2} \quad (5)$$

Here,  $S(d_c, d_s)$  is a correction factor that depends on the relative values of  $d_c$  and  $d_s$ . We calculated the exact value of  $S(d_c, d_s)$  for each particle, although in all cases, its value is very close to 1.<sup>4</sup> Figure 3c shows a distribution plot of particle diameter calculated according to eq 5 using the data shown in Figure 2b–d. The average particle diameter and its distribution at three different driving potentials are very similar to one another (Table 1), indicating the raw (current vs time) data are not distorted by signal filtering. The diameter of the smallest detectable particle was 28 nm. The important point is that the measured particle diameter determined by Coulter counting, which ranges from  $57 \pm 7$  to  $59 \pm 8$  nm, depending on  $E_M$ , our TEM measurements ( $61 \pm 9$  nm) and the methods used by the manufacturer ( $57 \pm 6$  nm) are in agreement.

The surface charge for each individual particle can be calculated according to eq 4 once its diameter is determined from the pulse height. Figure 3d shows that the surface charge,  $Q$ , is approximately proportional to the surface area of the particles, indicating that the area per surface charge ( $91 \pm 6$  nm<sup>2</sup>/charge, determined from the values of all the individual particles) is nearly constant. Moreover, the measured value of  $Q$  is independent of  $E_M$  (Table 1) and close to the area per surface –COOH group independently determined by the manufacturer:  $84.97$  nm<sup>2</sup>/–

COOH.<sup>18</sup> This means that nearly all the acid groups are deprotonated at pH 7.3. This is further supported by our preliminary observation that the surface charge at pH 9 is essentially the same as the value determined at pH 7.3.<sup>19</sup> The acid dissociation discussed here for low-density –COOH groups on a polystyrene sphere is very similar to that of mercaptoalkanoic acids present at dilute surface concentration on a gold surface ( $pK_a \sim 5$ ).<sup>20</sup> The agreement of the measured surface charge with the vendor-reported value confirms our initial assumption that the observed mobility arises solely from electrophoretic transport and that other mechanisms that might either increase or decrease the transport rate can, to a first approximation, be ignored. It should be emphasized, however, that the above discussion relies heavily on the validity of eq 3. Thus, it is helpful to look closely at some of the assumptions implied by this equation.

First, at an ionic strength of 0.1 M, the Debye length is  $\sim 1$  nm, which is much smaller than the probe radius (30 nm). This means that the Helmholtz–Smoluchowski approximation mentioned previously remains satisfied in our case. Second, the Debye–Hückel approximation also holds, because the surface  $\zeta$  potential ( $|\zeta| = 2$  mV) calculated using eq 6 and the surface –COOH density of IDC-PS is smaller than the thermal energy (25 mV).<sup>16</sup>

$$\zeta = \frac{2Q}{\epsilon d_s(1 + d_s/2d_D)} \quad (6)$$

Here,  $\epsilon$  is the dielectric constant of the solution. Finally, interactions between the channel wall and the probe particles are expected to increase the transport time, but at present, we do not have independent data to quantify the effects of such interactions. However, comparison of the electrophoretic mobility measured in this study with values measured for probe particles moving in the bulk solution will allow us to reliably answer this question.

The particle concentration can be determined from the counting frequency ( $J_s$ , Table 1) which, for electrophoretically dominant transport, is given by eq 7 ( $C_s$  is the particle concentration).<sup>1</sup>

$$J_s = \frac{\pi d_c^2}{4} \frac{\mu E_M}{I_c + 0.8d_c} C_s \quad (7)$$

Equation 7 predicts that the observed frequency is linearly proportional to  $E_M$ . The particle concentration determined from eq 7 and the aforementioned particle data (57-nm diameter and 119 surface charges per particle, which are averages determined from data obtained at the three values of  $E_M$ ), is  $3.8 \times 10^{11}$  particles/mL, which means the true particle concentration is only slightly smaller than the nominal concentration ( $5 \times 10^{11}$  particles/mL).

**Coulter Counting of Polystyrene Particles Having High Surface–COOH Density.** Polystyrene particles having a similar diameter but a much higher acid surface density (Bangs-PS:  $60 \pm 10$  nm diameter, 24 220 –COOH groups per particle), as

(16) Overbeek, J. T. G.; Wiersema, P. H. In *Electrophoresis: Theory, Methods and Applications*; Bier, M., Ed.; Academic Press: New York, 1967; Vol. 2, pp 1–52.

(17) Israelachvili, J. N. *Intermolecular and Surface Forces*, 2nd ed.; Academic Press: San Diego, 1992.

(18) Vanderhoff, J. W.; Van den Hul, H. J.; Tausk, R. J. M.; Overbeek, J. T. G. In *Clean Surfaces: Their Preparation and Characterization for Interfacial Studies*; Goldfinger, G., Ed.; Marcel Dekker: New York, 1970; pp 15–44.

(19) Ito, T.; Sun, L.; Crooks, R. M. Preliminary results.

(20) Dai, Z.; Ju, H. *Phys. Chem. Chem. Phys.* **2001**, *3*, 3769–3773.

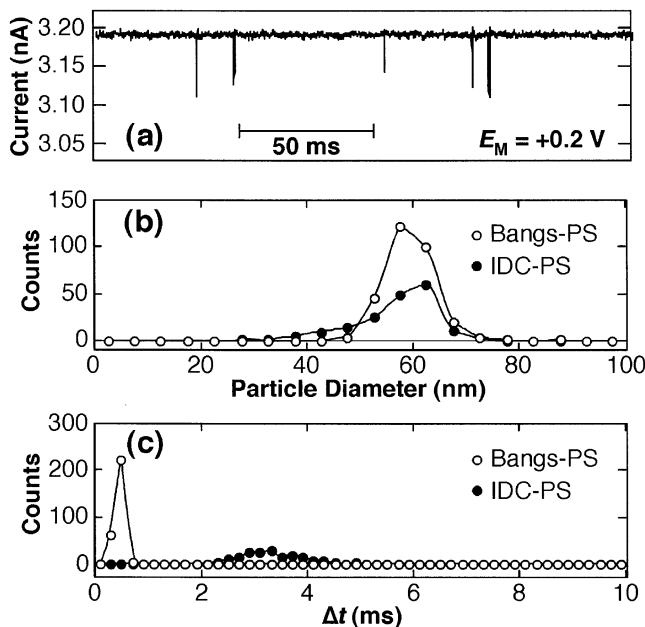


Figure 4. (a) Plot of current vs time obtained using a solution containing nominally  $5 \times 10^{11}$  Bangs-PS particles/mL, 0.1 M KCl, 10 mM  $\text{KH}_2\text{PO}_4/\text{K}_2\text{HPO}_4$  buffer (pH 7.3), and 0.1% (w/v) Triton X-100 at  $E_M = +0.2$  V. (b) Distribution of particle diameters for IDC-PS and Bangs-PS probes calculated from pulse height data at  $E_M = +0.2$  V. (c) Distribution of transport time ( $\Delta t$ ) for IDC-PS and Bangs-PS probes at  $E_M = +0.2$  V. In (b) and (c), the data were obtained using single-component solutions of either IDC-PS (filled circles) or Bangs-PS (open circles). The absolute number of counts in the distribution curves varies as a function of the total analysis time (Table 2).

Table 2. Diameter, Transport Time, Electrokinetic Surface Charge, and Counting Frequency for Bangs-PS Probes Determined from Coulter Counting Data

$E_M$ (V)	$N^a$ (time, s) <sup>e</sup>	$d_s$ (nm) <sup>b,c</sup>	$\Delta t$ (ms) <sup>c</sup>	$Q^{c,d}$	$J_s$ (s <sup>-1</sup> )
0.04	117 (53.2)	$55.5 \pm 4.3$	$2.4 \pm 0.4$ (0.08) <sup>f</sup>	$755 \pm 115$	2.2 (85) <sup>f</sup>
0.2	291 (16.7)	$59.2 \pm 4.7$	$0.5 \pm 0.2$ (0.02) <sup>f</sup>	$921 \pm 138$	17.4 (423) <sup>f</sup>
0.5	349 (7.18)	$56.1 \pm 5.0$	$0.2 \pm 0.0$ (0.008) <sup>f</sup>	$649 \pm 146$	48.6 (1058) <sup>f</sup>

<sup>a</sup> Total number of current pulses measured. <sup>b</sup> Particle diameter calculated using eq 5. <sup>c</sup> Average standard deviation. <sup>d</sup> Electrokinetic surface charge per particle calculated using eq 4. <sup>e</sup> Total time for each measurement. <sup>f</sup> Calculated using the number of surface -COOH groups provided by the manufacturer (24 220 per particle).

compared to the IDC-PS particles described previously ( $57 \pm 6$  nm, 120 -COOH groups per particle), were chosen as another standard for testing the MWNT-based Coulter counter. Figure 4a shows a typical current-vs-time plot for Bangs-PS at  $E_M = +0.2$  V. The average particle diameter for Bangs-PS, calculated from eq 5 and the pulse-height data (Figure 4b), is, within the standard deviation of the measurement, indistinguishable from that determined experimentally for IDC-PS; however,  $\Delta t$  for the two probes differs appreciably because of differences in surface charge (Figure 4c). A complete summary of the results of the analysis of Bangs-PS is provided in Table 2. One surprising result is that the surface charge determined using  $\Delta t$  (650–920 charges per particle) is only 3–4% of the acid surface density provided by the manufacturer (24 220 -COOH per particle). The observed count-

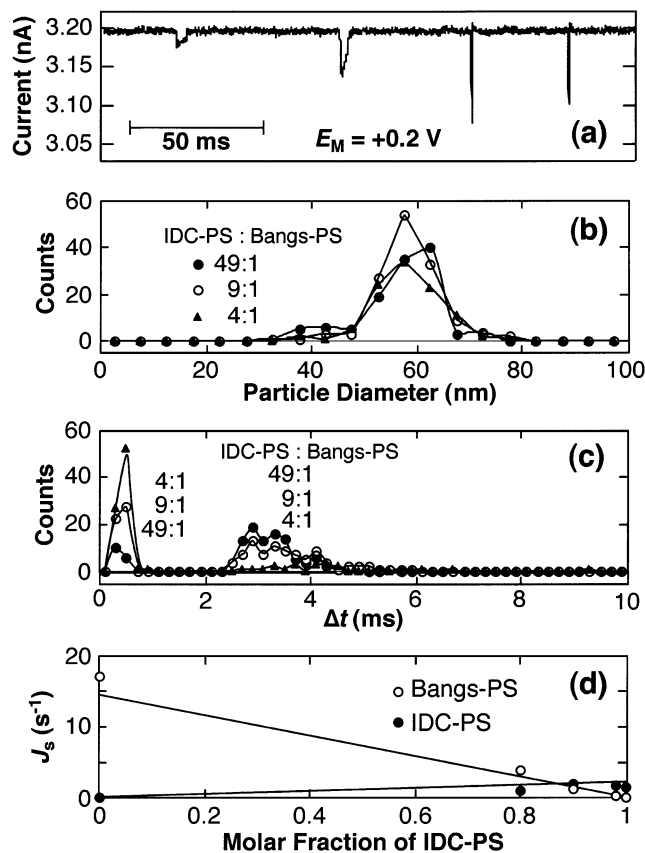


Figure 5. (a) Plot of current vs time at  $E_M = +0.2$  V obtained for a mixed solution containing a total of  $5 \times 10^{11}$  particles/mL of IDC-PS and Bangs-PS present at a molar ratio of 4:1, and 0.1 M KCl, 10 mM  $\text{KH}_2\text{PO}_4/\text{K}_2\text{HPO}_4$  buffer (pH 7.3), and 0.1% (w/v) Triton X-100. (b) Distribution of particle diameters, calculated from pulse heights, obtained at  $E_M = +0.2$  V using mixed solutions of IDC-PS and Bangs-PS at molar ratios of 49:1, 9:1, and 4:1. (c) Distribution of transport times ( $\Delta t$ ) calculated using the same set of raw data used in (b). (d) Relationship between particle-counting frequency and molar fraction of IDC-PS. The solid lines were calculated from the experimentally determined average particle diameters (57 nm for both IDC-PS and Bangs-PS), the electrokinetic surface charge obtained in this study (119 and 763 negative charges per particle for IDC-PS and Bangs-PS, respectively), and the nominal total particle concentration ( $5 \times 10^{11}$  particles/mL). Counts in the distribution plots are not normalized for the total analysis time, which is provided in Table 3.

ing frequency is also much smaller than that estimated from the number of surface -COOH groups provided by the manufacturer (Table 2). However, using the experimentally determined particle data for Bangs-PS (57 nm diameter and 763 surface charges per particle, which are averages determined from the entire data set at the three different values of  $E_M$ ), the value of  $J_s$ , and eq 7, we calculate a particle concentration of  $6.5 \times 10^{11}$  particles/mL, which is close to the nominal concentration of  $5 \times 10^{11}$  particles/mL. Thus, the experimental data are internally consistent.

We think the discrepancy between our measured surface charge density and the acid surface density provided by the manufacturer is attributable to some or all of the following three factors. First, when the surface charge density is high, the Debye-Hückel approximation underpinning eq 4 is expected to fail. However, at present, we have not numerically evaluated the likely error introduced by this failure of the approximation. Second, the effective surface charge can be smaller than the total number of

Table 3. Diameter, Transport Time, Electrokinetic Surface Charge, and Counting Frequency for the Mixture of IDC-PS and Bangs-PS Probes Determined from Coulter Counting Data ( $E_M = +0.2$  V)

IDC-PS/Bangs-PS	$N^a$ (time, s) <sup>e</sup>	$d_s$ (nm) <sup>b,c</sup>	$\Delta t$ (ms) <sup>c</sup>	$Q$ <sup>c,d</sup>	$J_s$ (s <sup>-1</sup> )
49:1					
IDC-PS	102 (62.5)	$57.4 \pm 7.7$	$3.3 \pm 0.6$	$119 \pm 37$	1.6
Bangs-PS	16 (62.5)	$52.4 \pm 8.7$	$0.4 \pm 0.1$	$821 \pm 234$	0.3
9:1					
IDC-PS	85 (41.6)	$59.5 \pm 7.0$	$3.5 \pm 0.7$	$121 \pm 37$	2.0
Bangs-PS	51 (41.6)	$56.5 \pm 4.8$	$0.4 \pm 0.0$	$926 \pm 129$	1.2
4:1					
IDC-PS	21 (21.3)	$58.1 \pm 7.8$	$4.4 \pm 1.5$	$100 \pm 42$	1.0
Bangs-PS	82 (21.3)	$58.2 \pm 6.3$	$0.4 \pm 0.1$	$898 \pm 174$	3.8

<sup>a</sup> Total number of current pulses measured. <sup>b</sup> Particle diameter calculated using eq 5. <sup>c</sup> Average standard deviation. <sup>d</sup> Electrokinetic surface charge per particle calculated using eq 4. <sup>e</sup> Total time for each measurement.

-COOH functional groups, especially at a high surface-packing density. In other words, at pH 7.3, the acid groups may not completely deprotonate because their  $pK_a$  shifts to a higher value ( $pK_a = 6-9$  in acid-terminated self-assembled monolayers).<sup>20,21</sup> However, this factor may not be so significant, because our preliminary results showed that the area per surface charge for Bangs-PS at 7.3 is very similar to that determined at pH 9.<sup>19</sup> Finally, the effective surface charge can also be lowered significantly by positively charged counterions nonspecifically associated with the negatively charged carboxylate groups (in the diffuse layer) or specifically adsorbed via strong chemical binding, such as binding with metal cations<sup>21</sup> or binding of  $K^+$  promoted by surface-confined Triton-X100 surfactant molecules.<sup>1</sup> For highly charged particles, this effect is known as ionic screening.<sup>22,23</sup> It should be pointed out that, strictly speaking, the surface charge measured by the Coulter counting method as described in this work is really an electrokinetic charge, which is the sum of charges contributed from all species, whether positive or negative, located within the hydrodynamic shear plane of the particle. In most cases, the space enclosed by this plane is larger than the space physically occupied by a particle because, when set in motion, a charged particle almost always drags molecules, such as solvent and counterions, along with it. More experiments are required to clarify the origin of the observed discrepancy in surface charge.

**Detection of Polystyrene Nanoparticles Having the Same Size but Different Surface Charge Density.** The clear difference between the surface charge (or transport time) for Bangs-PS and IDC-PS probes suggests that it should be possible to discriminate between them in a mixed solution. To test this hypothesis, we prepared three different mixtures having IDC-PS/Bangs-PS ratios of 49:1, 9:1, and 4:1, while keeping the total nominal concentration constant at  $5 \times 10^{11}$  particles/mL. Figure 5a shows a typical current-vs-time plot for the 4:1 ratio, and Figure 5b and 5c show distribution plots of particle diameter and transport time, respectively. The results are summarized in Table 3. Figure 5a shows two types of signals having wider (2 signals on the left) and narrower (2 signals on the right) width. It is clear that it is not possible to distinguish the two probes on the basis of their diameters (Figure 5b), but they can be differentiated on the basis

of their charge difference (Figure 5c). Note that the relative heights of the two peaks in Figure 5c depend on the molar ratio of the two probes. Figure 5d shows the counting frequencies of Bangs-PS and IDC-PS in solution as a function of mole fraction. If there is no interaction between particles, then the total frequency,  $J_{s,\text{total}}$ , of the mixed solution containing particles 1 (concentration:  $C_{s,1}$ ) and 2 (concentration:  $C_{s,2}$ ) is given by eq 8.

$$J_{s,\text{total}} = \frac{C_{s,1}}{C_{s,0}} J_{s,1} + \frac{C_{s,2}}{C_{s,0}} J_{s,2} \quad (8)$$

Here,  $C_{s,0}$  is the total particle concentration ( $= C_{s,1} + C_{s,2}$ ), and  $J_{s,1}$  and  $J_{s,2}$  are the counting frequencies for particles 1 and 2 in their single-component solutions at the concentration  $C_{s,0}$ . This equation predicts that the counting frequency is linearly related to the mole fraction of the individual components. Indeed, Figure 5d shows that plots of the frequencies of the two nanoparticles lie on lines derived from eqs 7 and 8 and their experimentally determined  $Q$  and particle size. These results clearly show that the MWNT-based Coulter counter discriminates between nanoparticles having different surface charges and correctly provides their concentrations.

## SUMMARY AND CONCLUSIONS

The results described here demonstrate that Coulter counting based on single-pore MWNT channels provides a means to simultaneously determine the size and electrokinetic surface charge of individual nanoparticles when transport through the channel is dominated by electrophoresis. Coulter counting is a powerful analysis method, because it is an intrinsically stochastic approach and, thus, provides a statistical analysis of the properties of an ensemble of particles, which is not always possible for other types of analytical methods. We anticipate that MWNT-based Coulter counters will be useful for fundamental studies of colloids and mass transport phenomena in nanoporous media.<sup>3</sup> In the future it may be possible to reduce the nanotube diameter sufficiently to detect proteins and other important biological analytes.

## ACKNOWLEDGMENT

We gratefully acknowledge financial support from the U. S. Department of Energy (Contract no. DE-FG03-01ER15247). We

(21) Kokkoli, E.; Zukoski, C. F. *Langmuir* **2000**, *16*, 6029-6036.

(22) Roberts, J. M.; O'Dea, J. J.; Osteryoung, J. G. *Anal. Chem.* **1998**, *70*, 3667-3673.

(23) Bacquet, L.; Trizac, E.; Aubouy, M. *J. Chem. Phys.* **2002**, *117*, 8138-8152.

thank Drs. Hagan Bayley, Orit Braha, LiQun Gu, and William Lackowski for their suggestions relating to noise reduction, and Drs. Zhiping Luo and E. Ann Ellis (Microscopy and Imaging Center, Texas A&M University) for their assistance with TEM imaging. We also thank Dr. D. G. Glasgow (Applied Sciences, Inc., Cedarville, OH) for providing the carbon nanotubes used in this study. We thank Prof. Henry S. White (University of Utah) and his students for suggestions related to fabrication of the PDMS support.

#### SUPPORTING INFORMATION AVAILABLE

TEM images of MWNTs supported on TEM grids and of a representative membrane containing a MWNT channel. This information is available free of charge via the Internet at <http://pubs.acs.org>.

Received for review January 24, 2003. Accepted March 27, 2003.

AC034072V